

# Effect of uniform distributions of bonded and debonded fibers on the growth of the fiber/matrix interface crack in UD laminates with different fiber contents under transverse loading

Luca Di Stasio<sup>a,b</sup>, Janis Varna<sup>b</sup>, Zoubir Ayadi<sup>a</sup>

<sup>a</sup>Université de Lorraine, EEIGM, IJL, 6 Rue Bastien Lepage, F-54010 Nancy, France

<sup>b</sup>Luleå University of Technology, University Campus, SE-97187 Luleå, Sweden

---

## Abstract

*Priority: 1*

*Target journal(s):* Composites Part B: Engineering, Composites Part A: Applied Science and Manufacturing, Composite Structures, Journal of Composite Materials, Composite Communications

---

## 1. Introduction

1. We start with a few lines devoted to the spread tow technology and thin plies: what they are, what can be done, what are the possible applications.
- 5 2. By quoting the relevant references, we report on the observation that one of the main beneficial mechanisms in thin ply is the retardation of transverse crack propagation. We then enlarge by reporting the microscopical observations by Saito, in which debonds where also observed. We observe that available microscopic observations are just a few and mainly in 2D.
- 10 3. Propagation of transverse cracks has been widely investigated both analytically and numerically
4. Initiation at the level of fiber/matrix interface is instead a less researched subject.

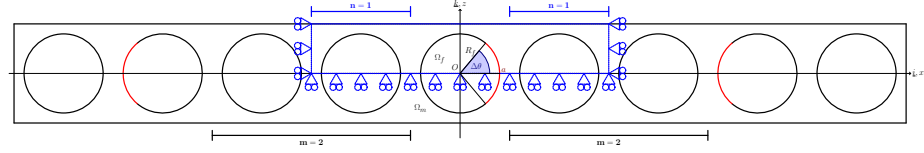
5. cohesive elements are a possible choice, but have some drawbacks, which  
15 makes a LEFM approach valuable
6. With regard to LEFM studies of laminates under transverse loading, models can be found in the literature about: the single fiber in infinite matrix under different mode of loading, the effect of adjacent fibers on a fiber in infinite matrix under different mode of loading, the single fiber in an  
20 equivalent composite in transverse tension, the effect of adjacent fibers on a fiber in an equivalent composite in transverse tension.
7. For initiation of transverse cracking at the fiber/matrix interface in UD laminates under transverse tension, there is thus a gap regarding: the effect of fiber volume fraction; the interaction of debonded and bonded  
25 fibers in micro-structured assemblies, i.e. no homogenization. This article addresses these two points.
8. We conclude the introduction with a summary of the article's structure.

## 2. RVE models & FE discretization

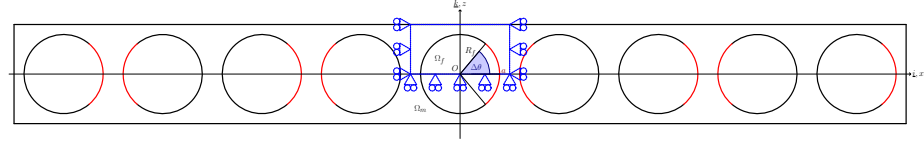
### 2.1. Models of Representative Volume Element (RVE)

30 In order to investigate the interaction between debonds in UD composites, we developed different models of laminates in which the only damage present is represented by the fiber/matrix interface crack. All of these Representative Volume Elements feature regular microstructures with fibers placed according to a square-packing tiling. Laminates are considered to be plane and infinite  
35 to all practical purposes in their own plane, i.e. along laminate axes  $x$  and  $y$ . This allows the use of 2D models under the assumption of plane strain, defined in the  $x - z$  section of the laminate. Consequently, debonds are considered to be fully developed along the length of the respective fiber, corresponding to the  $y$  laminate axis or laminate's width, but only partially along the surface of the  
40 fiber, i.e. the circumferential direction. The analysis presented thus applies to long debonds, of which we are interested in understanding the mechanisms of

growth along the surface of the fiber. Laminates are further supposed to be subjected to transverse tension, applied along the  $x$  direction in the pictures.



(a) Single layer of fibers with a debond appearing every  $m$  fibers.

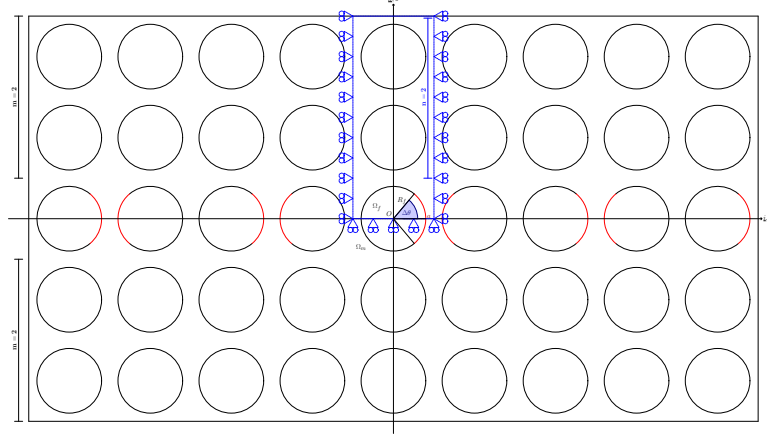


(b) Single layer of fibers with debonds appearing on each fiber.

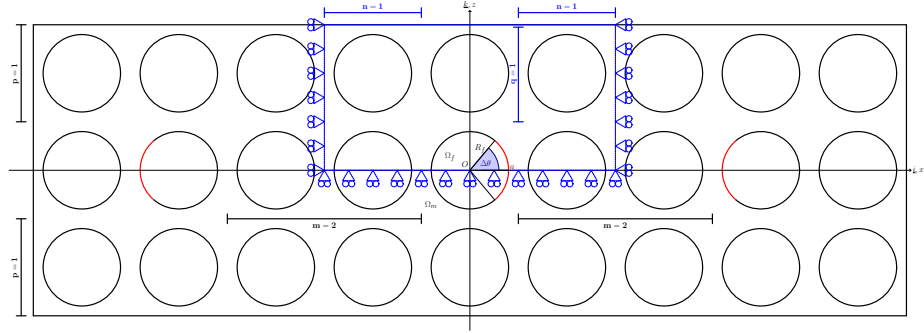
Figure 1: Models of UD laminates with a single layer of fibers and debonds repeating at different distances. The corresponding repeating element (RVE) is highlighted in blue.

The first two models feature, as shown in Fig. 1, a UD laminate with only  
 45 one layer of fibers across its thickness. This is quite an extreme model from  
 the microstructural point of view; however, it allows to focus the analysis on  
 the interaction between debonds placed along the direction of the load. In  
 retrospective, if only 20 years ago such a model would have been considered too  
 abstracted from the physical reality, the recent advancements in the spread tow  
 50 technology make this approach appealing also for practical considerations. In  
 the first version of the model laminate, Fig. 1a, debonds appear in the laminate  
 every  $m$  fibers on alternating sides of the debonded fiber. The symmetries of  
 the model allow the use of a Repeating Unit Cell (RUC), represented in blue  
 in 1a, with a central debonded fiber and  $n = \frac{m}{2}$  fiber(s) on each side. Symmetry  
 55 is applied on the lower boundary and kinematic coupling conditions on the left  
 and right sides. The upper surface is left free. In the following, this model will  
 be referred to as  $n$  fiber(s) on each side. In the second version of the single-layer-  
 of-fibers model, 1b, a debond appears on each fiber on alternating sides. The  
 corresponding RUC has only one debonded fiber, with symmetry on the lower  
 60 side and kinematic coupling on the left and right ones. The upper boundary is

again free. We will refer to this model as *free*.



(a) Multiple layers of fibers with debonds appearing on each fiber belonging to the central layer.



(b) Multiple layers of fibers with a debond appearing every  $m$  fibers within the central layer.

Figure 2: Models of UD laminates with different layers of fibers and debonds repeating at different distances. The corresponding repeating element (RVE) is highlighted in blue.

The second set of models considers instead laminates with multiple layers of fibers across the thickness: a finite number of layers in the first two models ( 2a and 2b); an infinite number in the model of Fig. 3. In the first model (Fig. 2a) all the fibers in the central layer are debonded.  $m$  layers are present above and below this central layer, corresponding to a RUC with  $n = m$  fibers above. This model will be referred to in the following as  $n$  fibers above. In the second model

(Fig. 2b), a debond appear every  $m$  fiber(s) in the central line of fibers in a laminate with  $p$  layers. The corresponding RUC has thus  $n = \frac{m}{2}$  fiber(s) on  
70 each side and  $q = p$  above. We will refer to this model as  $n$  fibers on each side,  
 $q$  above.

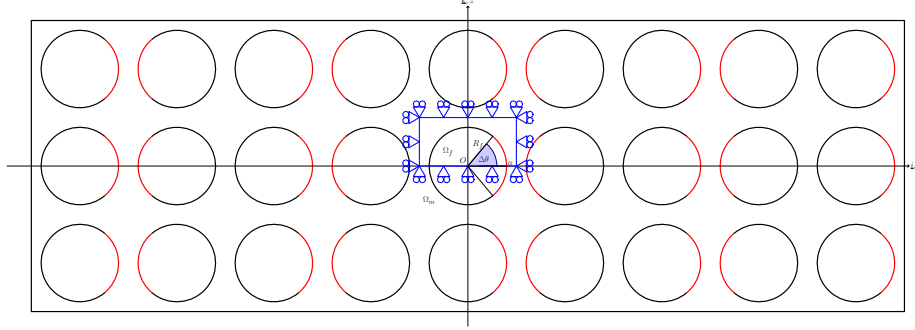


Figure 3: Model of UD laminates with an infinite number of layers of fibers and debonds appearing on each fiber. The corresponding repeating element (RVE) is highlighted in blue.

Finally, the last model considers a laminate with an infinite number of fibers across the thickness, all with a debond at their interface. The corresponding RUC is made by a single fiber with a debond and kinematic coupling conditions  
75 applied to upper boundary. This model is referred to as *coupling*. For all these three models, the corresponding RUC possesses symmetry on the lower boundary, and kinematic coupling is applied on the left and right sides.

## 2.2. Finite Element (FE) discretization

Each RUC is discretized using the Finite Element Method (FEM) within  
80 the Abaqus environment, a commercial FEM package. The length  $l$  and height  $h$  of the model (see Fig. 4a) are determined by number of fibers  $n$  present on the side and the number of layers  $q$  above the central line of fibers (see 2.1) according to Eq. 1:

$$l = (2n + 1) L \quad h = (2q + 1) L; \quad (1)$$

where the reference length  $L$  is defined as a function of the fiber volume  
85 fraction  $V_f$  and the fibers' radius according to

$$L = \frac{R_f}{2} \sqrt{\frac{\pi}{V_f}}. \quad (2)$$

The relationships in Eqs. 1 and 2 ensure that the local and global  $V_f$  are everywhere equal.

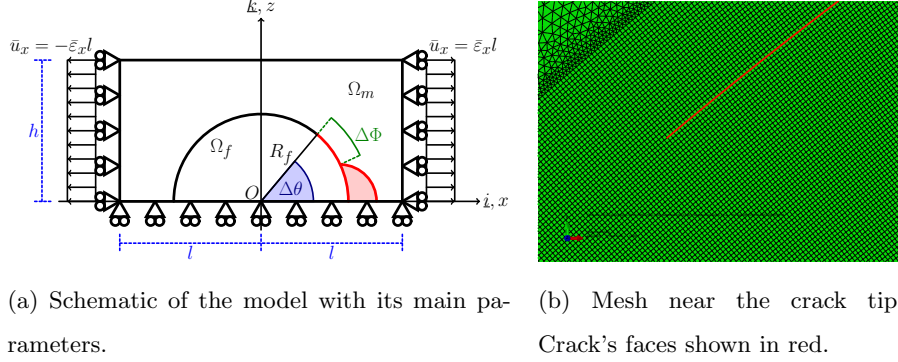


Figure 4: Details and main parameters of the Finite Element model.

The debond is placed symmetrically with respect to the  $x$  axis (in red in 4a) and has an angular size of  $\Delta\theta$  (the full debond's size is thus  $2\Delta\theta$ ). For high debond's sizes ( $\geq 60^\circ - 80^\circ$ ), a region of variable size  $\Delta\Phi$  appears at the crack tip in which the crack's faces are in contact and slide on each other. Due to its appearance, frictionless contact is considered between the two crack's faces to allow free slipping and avoid interpenetration. Symmetry with respect to the  $x$  axis is applied on the lower boundary and kinematic coupling on the left and right sides. The upper boundary is in general free, except for the model coupling (Fig. 3) which requires kinematic coupling also on the upper side. Constant transverse strain  $\bar{\varepsilon}$  equal to 1% is applied to the right and left sides by means of an imposed displacement of, respectively,  $\pm\bar{\varepsilon}l$ .

The model is meshed using second order, 2D, plane strain triangular CPE6 and rectangular CPE8 elements. A regular mesh of quadrilateral elements with an almost unitary aspect ratio is required at the crack tip, as shown in Fig. 4b. The angular size  $\delta$  of an element in the crack tip region is always equal to  $0.05^\circ$ . The mode I, mode II and total Energy Release Rates (ERRs) represent the

main output of the FEM analysis; they are evaluated using the VCCT technique  
 105 implemented in a custom Python routine and, for the total ERR, the J-integral  
 by application of the Abaqus built-in functionality. A glass fiber-epoxy system  
 is considered in every model, and the properties used are listed in Table 1.

Table 1: Summary of the mechanical properties of fiber and matrix.

| <b>Material</b> | $E$ [GPa] | $G$ [GPa] | $\nu$ [-] |
|-----------------|-----------|-----------|-----------|
| Glass fiber     | 70.0      | 29.2      | 0.2       |
| Epoxy           | 3.5       | 1.25      | 0.4       |

### 2.3. Validation of the model

The model is validated in Fig. 5 against the results reported in ??, obtained  
 110 with the Boundary Element Method (BEM) for a single fiber with a symmetric  
 debond placed in an infinite matrix. This situation is modeled using the *free*  
 RVE with  $V_f = 0.0079\%$ , which corresponds to a RUC's length and height of  
 $\sim 100$ .

To allow for a comparison, the results are normalized following ?? with  
 115 respect to a reference Energy Release Rate  $G_0$  defined as

$$G_0 = \frac{1 + k_m}{8\mu_m} \sigma_0^2 \pi R_f \quad (3)$$

where  $\mu$  is the shear modulus,  $k_m$  is the Kolosov's constant defined as  $3 - 4\nu$   
 for plane strain conditions,  $R_f$  is the fiber radius and the pedix  $m$  refers to  
 the properties of the matrix.  $\sigma_0$  is the stress at the boundary, computed as  
 the average of the stress extracted at each boundary node along the right side  
 120 (arithmetic average as nodes are equispaced by design along both the left and  
 right sides).

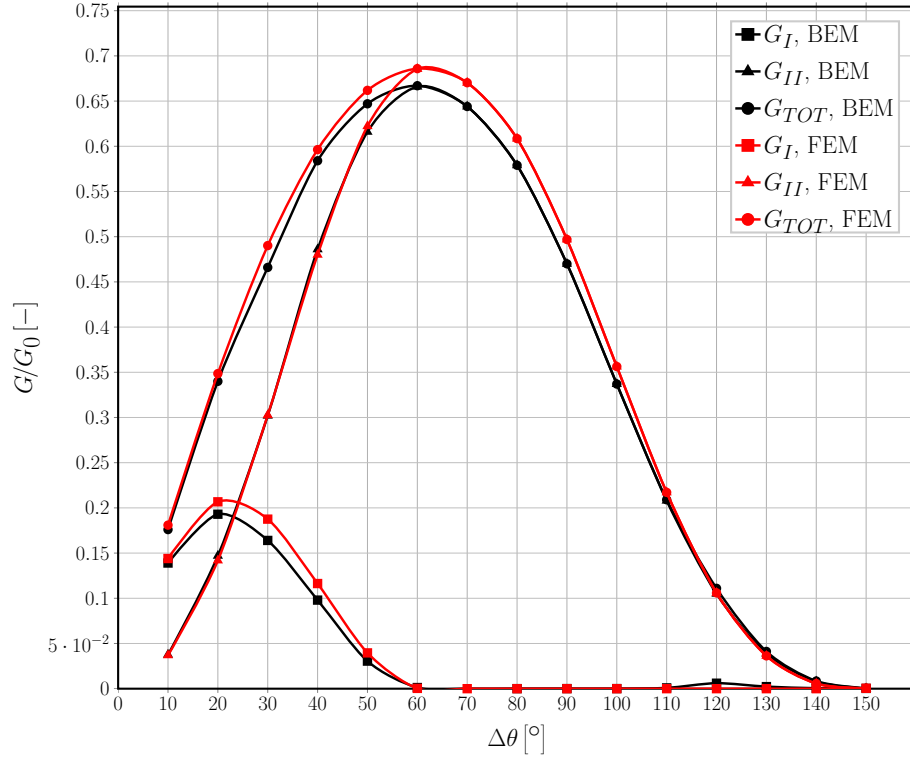


Figure 5: Validation of the single fiber model for the infinite matrix case with respect to the BEM solution in [].

### 3. Results & Discussion

#### 3.1. Effect of Fiber Volume Fraction

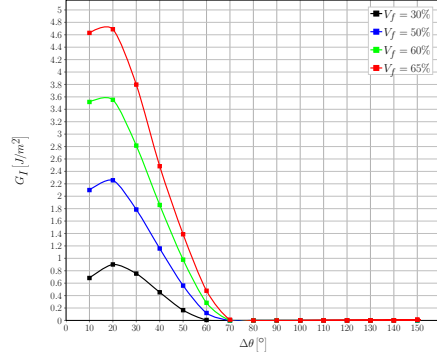
The effect is similar for all the different BC cases, it's enough to show some of them to exemplify.  $G_I$  in Fig. 6,  $G_{II}$  in Fig. 7.

Graphics of ERR vs  $\Delta\theta$ , one curve for each  $V_f$ , one graphic for each selected BC. Selected BC: free, coupling, some examples with fibers (see captions).

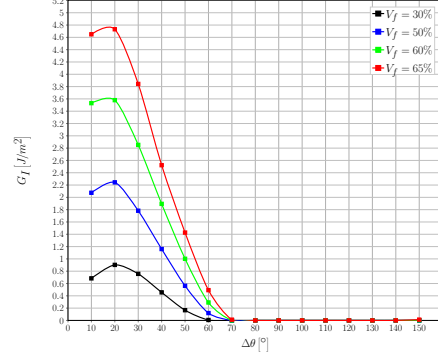
#### 3.2. Interaction between debonds in UD laminates with a single layer of fibers

We start with a simpler (1 parameter: number of fibers in the horizontal directions) but more extreme model: one line of fibers. What's the effect on  $G_I$  and  $G_{II}$ ? It increases them: a compliant element in the middle of two stiffer ones. Reference to Kies strain magnification.  $G_I$  in Fig. 8,  $G_{II}$  in Fig. 9.



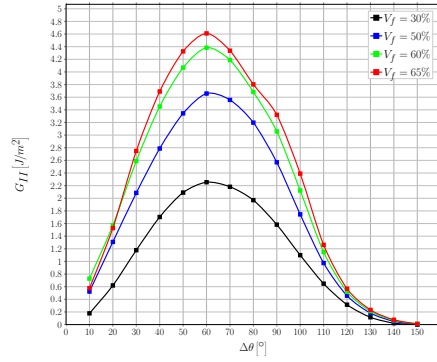


(a) 5 fibers each side, 5 above.

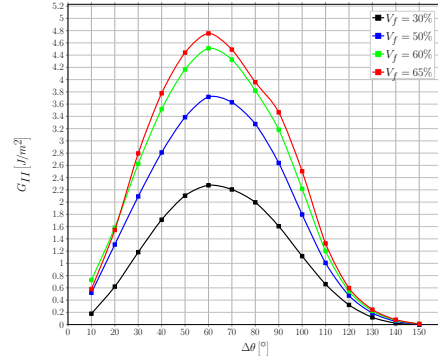


(b) 10 fibers each side, 10 above.

Figure 6: A view of the effect of fiber volume fraction on Mode I ERR in two exemplificative models.



(a) 5 fibers each side, 5 above.



(b) 10 fibers each side, 10 above.

Figure 7: A view of the effect of fiber volume fraction on Mode II ERR in two exemplificative models.

One graphic for each  $V_f$  (30%,50%,60%,65%), one curve for each case of fibers on the side (1, 2, 3, 5, 10, 50, 100).

135

### 3.3. Influence of layers of fully bonded fibers on debond's growth in a centrally located line of debonded fibers

We then move to a ply with multiple lines of fibers and only debonded fibers in the central one (still only 1 parameter: number of fibers in vertical direction,

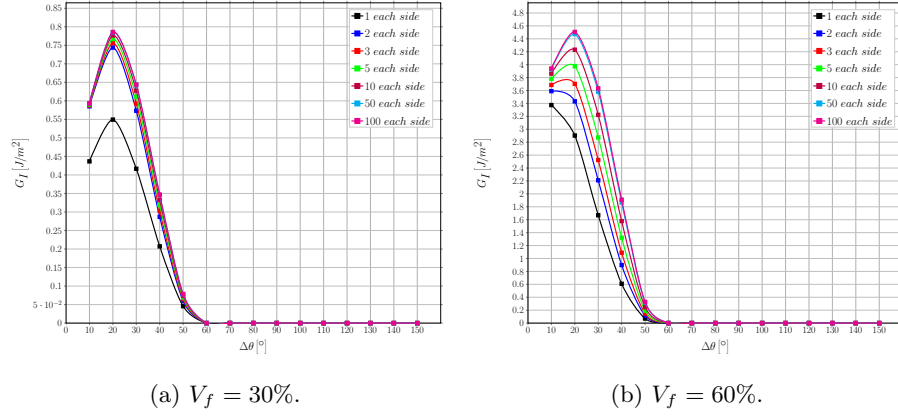


Figure 8: Effect of the interaction between debonds appearing at regular intervals on Mode I ERR in a single-ply laminate with a single layer of fibers at different levels of fiber volume fraction  $V_f$ .

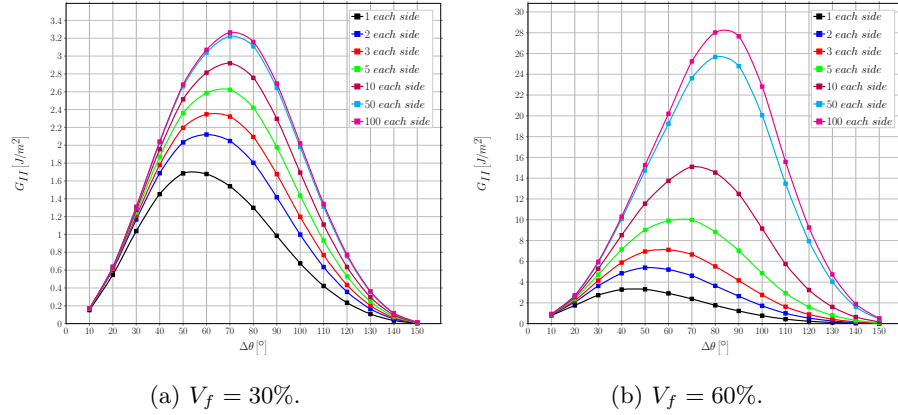


Figure 9: Effect of the interaction between debonds appearing at regular intervals on Mode II ERR in a single-ply laminate with a single layer of fibers at different levels of fiber volume fraction  $V_f$ .

140 but bit closer to real plies). No significant effect.  $G_I$  in Fig. 10,  $G_{II}$  in Fig. 11.

One graphic for each  $V_f$  (30%,50%,60%,65%), one curve for each case of fibers on top (1, 2, 3, 5, 10, 50, 100).

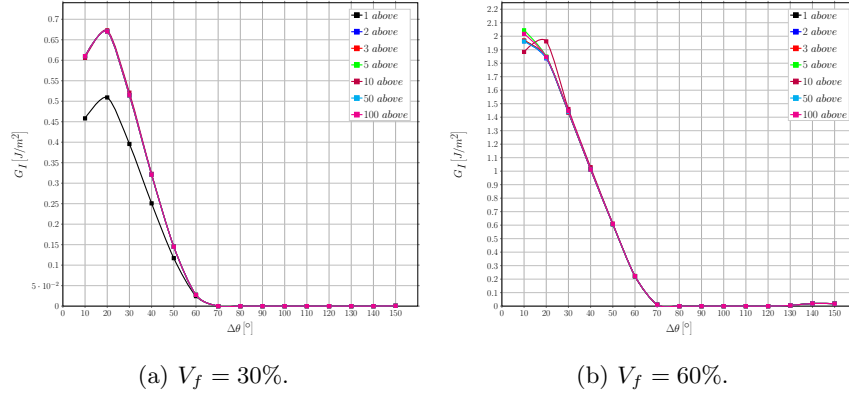


Figure 10: Influence of layers of fully bonded fibers on debond's growth in Mode I ERR in a centrally located line of debonded fibers at different levels of fiber volume fraction  $V_f$ .

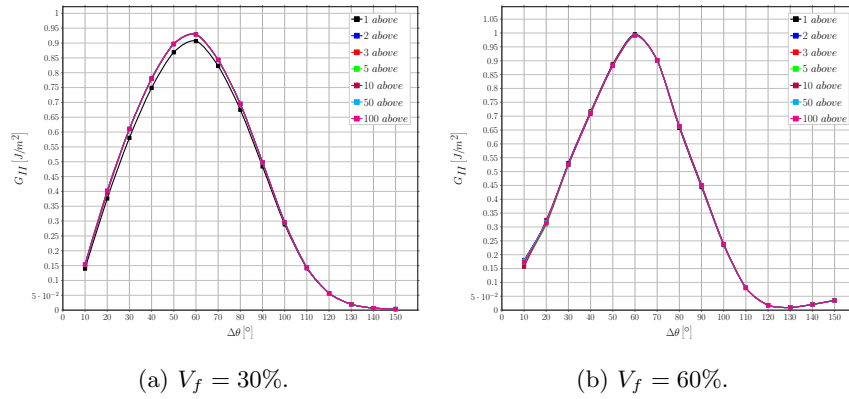


Figure 11: Influence of layers of fully bonded fibers on debond's growth in Mode II ERR in a centrally located line of debonded fibers at different levels of fiber volume fraction  $V_f$ .

### 3.4. Interaction between debonds in UD laminates with multiple layers of fibers

145 Finally models that are closer to real laminates and are more complex (2 parameters: number of fibers along the horizontal direction, number of layers in the vertical one).  $G_I$  in Fig. 12,  $G_{II}$  in Fig. 13.

One graphic for each  $V_f$  (30%,50%,60%,65%), one curve for some selected case of fibers on top and on the side. Hypothesis of selected cases ([n. on side, 150 n. on top]): [1,1], [2,1], [2,2], [5,1], [5,5], [10,1], [10,10], [50,1], [50,10], [100,1], [100,10]

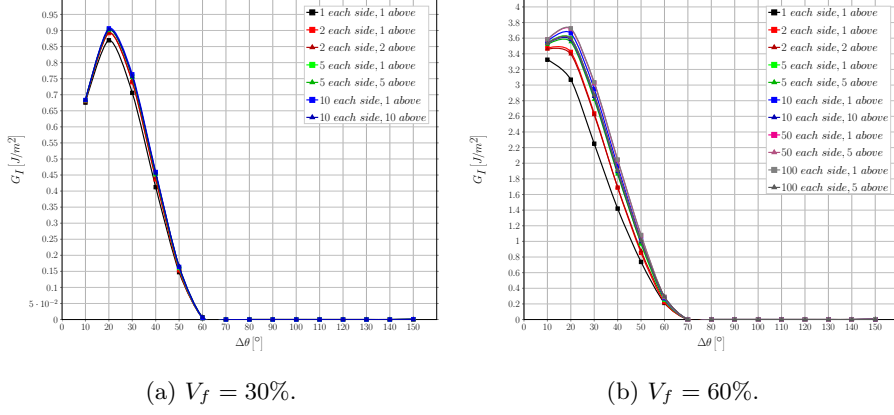


Figure 12: Effect of the interaction between debonds appearing at regular intervals on Mode I ERR in a single-ply laminate with multiple layers of fibers at different levels of fiber volume fraction  $V_f$ .

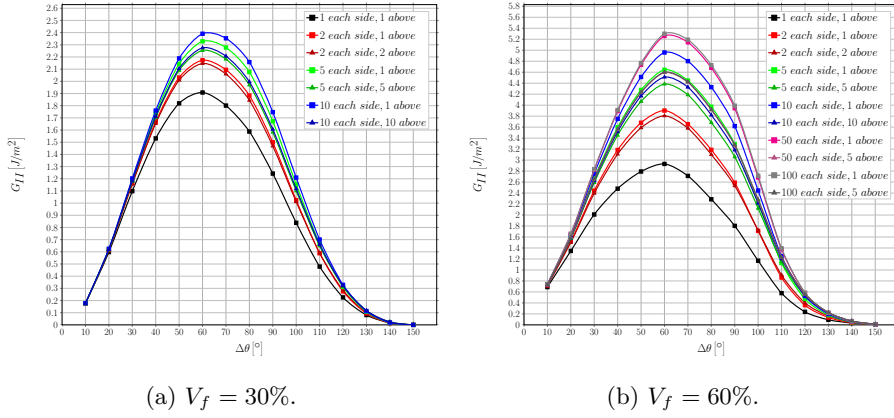


Figure 13: Effect of the interaction between debonds appearing at regular intervals on Mode II ERR in a single-ply laminate with multiple layers of fibers at different levels of fiber volume fraction  $V_f$ .

### 3.5. Comparison with the single fiber model with equivalent boundary conditions

We compare the previous results with the corresponding models of single fibers with equivalent BC. We draw conclusions on the possibility of using a

single fiber with equivalent BCs. By remembering the actual ply configurations the repeating elements are modeling, and observing that in the vertical direction no significant effect related to the presence of debonded or bonded fiber can be found, we conclude that debonds appearing in fibers aligned in the vertical direction are energetically equivalent, and thus different configurations of debonded/bonded fibers along the vertical direction have the same probability. It is thus likely, from the energetic point of view, that debonds form at the same time along fibers aligned vertically.  $G_I$  in Fig. 14 and Fig. 16,  $G_{II}$  in Fig. 15 and Fig. 17.

One graphic for each  $V_f$  (30%,50%,60%,65%), one curve for single fiber with BC + some selected case of fibers on top and on the side. Hypothesis of selected cases ([n. on side, n. on top]): [1,1], [2,1], [2,2], [5,1], [5,5], [10,1], [10,10]

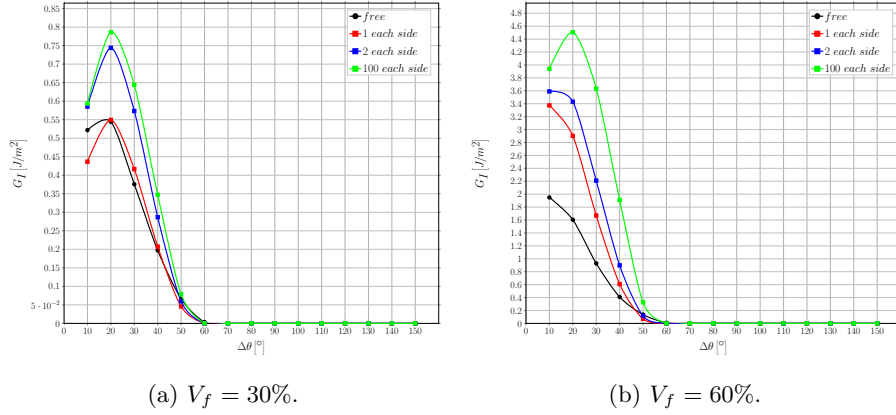


Figure 14: Comparison of Mode I ERR between the single fiber model with free upper boundary and the multiple fibers model with fibers only on the side at different levels of fiber volume fraction  $V_f$ .

#### 4. Conclusions & Outlook

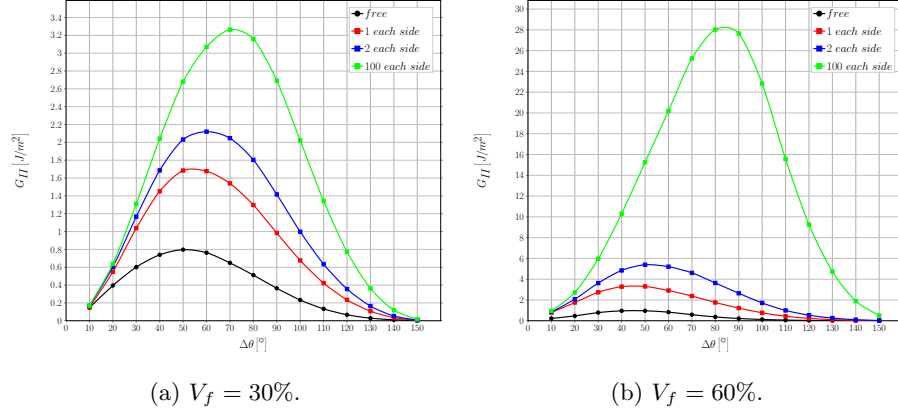


Figure 15: Comparison of Mode II ERR between the single fiber model with free upper boundary and the multiple fibers model with fibers only on the side at different levels of fiber volume fraction  $V_f$ .

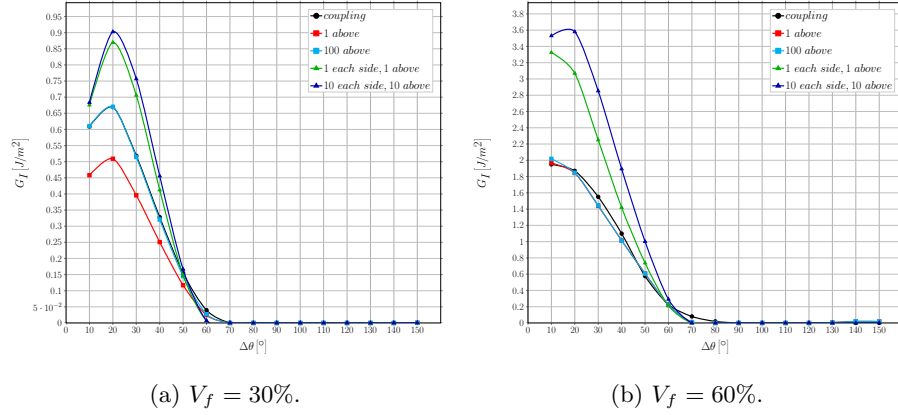
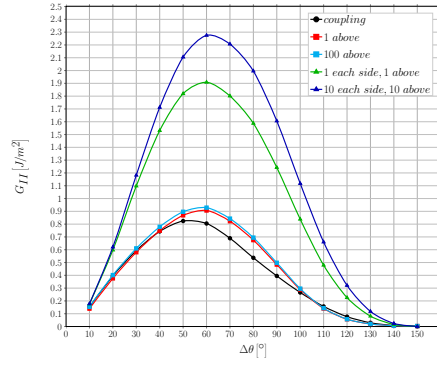
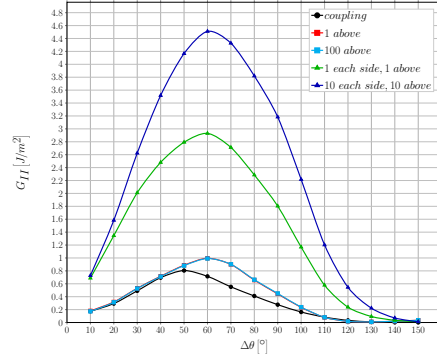


Figure 16: Comparison of Mode I ERR between the single fiber model with coupling conditions along the upper boundary and the multiple fibers model with fibers above and both above and on the side at different levels of fiber volume fraction  $V_f$ .



(a)  $V_f = 30\%$ .



(b)  $V_f = 60\%$ .

Figure 17: Comparison of Mode II ERR between the single fiber model with coupling conditions along the upper boundary and the multiple fibers model with fibers above and both above and on the side at different levels of fiber volume fraction  $V_f$ .